Assessing texturometer-derived rheological data for predicting the printability of gummy formulations in SSE 3D printing

Morenikeji Aina, Fabien Baillon, Romain Sescousse, Noelia M. Sanchez-Ballester, Sylvie Bégu, Ian Soulairol, Martial Sauceau

International Journal of Pharmaceutics 662 (2024) 124471

Contents lists available at ScienceDirect

International Journal of Pharmaceutics

journal homepage: www.elsevier.com/locate/ijpharm

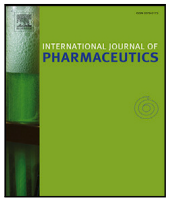

Assessing texturometer-derived rheological data for predicting the printability of gummy formulations in SSE 3D printing

Morenikeji Aina [a,*], Fabien Baillon [a], Romain Sescousse [a], Noelia M. Sanchez-Ballester [b,c], Sylvie Begu [b], Ian Soulairol [b,c], Martial Sauceau [a]

[a] RAPSODEE, IMT Mines Albi, CNRS, University of Toulouse, 81013 Albi, France
[b] ICGM, University of Montpellier, CNRS, ENSCM, Montpellier, France
[c] Department of Pharmacy, Nîmes University Hospital, Nîmes, France

ARTICLE INFO

Dataset link: pythonanywhere.com

Keywords:
Rheology
Texturometer
Capillary rheometer
Rotational rheometer
Semi-solid extrusion
Flow behaviour

ABSTRACT

Semi-solid extrusion (SSE), an additive manufacturing technique, is gaining significant attention for the printing of thermosensitive drugs. Hydrogels, one of the materials used in SSE, have emerged as a focus in pharmaceutical applications due to their ability to control the release of therapeutic agents spatially and temporally. Understanding the non-Newtonian flow and evaluating the mechanical properties of hydrogel-based materials during extrusion is, however, essential for successful 3D printing. Thus, users often find themselves conducting both rheological and texture profile analyses to characterize the hydrogel. While texturometers are primarily used to evaluate mechanical or sensory properties, viscosity measurements are typically performed using rotational rheometers or viscometers. In this study, we demonstrated how comparable rheological information can be obtained using a texturometer as a capillary rheometer. By preparing similar formulations to a previous study, we compared the rheological data obtained from a rotational rheometer to the data obtained from the texturometer. The means of the parameters obtained by fitting the data from both techniques to the power law model showed insignificant differences. In addition, three clusters were formed based on the flow behaviour and printability of the samples using principal component analysis. Furthermore, the printability was predicted using the samples' consistency and flow indexes, and the regression coefficient was 96.62 and 60.03% for capillary and rotational flow parameters, respectively. This approach thus holds the potential to streamline the time, expertise and equipment required for the rheological characterization of hydrogels for applications in semi-solid extrusion.

1. Introduction

Additive manufacturing (AM), also known as three-dimensional (3D) printing, is a technology that enables three-dimensional structures and components layer by layer from a 3D model or digital file. 3D printing (3DP) has been widely and successfully applied in diverse fields due to its unique features, such as rapid prototyping, production of complex structures, and customized and personalized products (Iftekar et al., 2023). In the pharmaceutical industry, the ability to produce more complex, on-demand products, as well as the ability to personalize the treatment (or dose), make 3D printing particularly interesting for paediatric formulations (Cui et al., 2021). The American Society of Testing Materials (ASTM) has classified 3D printing technologies into 7 main categories: material jetting, binder jetting, powder bed fusion, VAT polymerization, material extrusion, sheet lamination, and direct energy deposition (Saleh Alghamdi et al., 2021). All but 2 (sheet lamination and direct energy deposition), are used today in the pharmaceutical industry. There has however been increased interest in the use of semi-solid extrusion (SSE), a type of material extrusion 3DP technique, due to its low-temperature processing and the use of semi-solid which differentiates it from other material extrusion techniques such as Fused Deposition Moulding (FDM) and direct powder extrusion (DPE) (Seoane-Viaño et al., 2021). The use of low heat also reduces the risk of drug instability, and the possibility to use a wider range of excipients as feedstock materials to obtain gels or pastes for the 3D printing process (Lysyk Funk et al., 2023).

When combined with SSE, hydrogels have emerged as a promising material that allows the creation of soft-material with 3D structures, that are printable at room temperature and customized by tuning the geometric design and/or the formulation components (Bom et al., 2022). Indeed, the 3D structures of these polymers, linked together

* Corresponding author.
E-mail address: morenikeji.aina@mines-albi.fr (M. Aina).

https://doi.org/10.1016/j.ijpharm.2024.124471
Received 10 June 2024; Received in revised form 10 July 2024; Accepted 11 July 2024
Available online 15 July 2024

by supramolecular interactions or covalent bonds, enable them to absorb and retain enormous quantities of aqueous material, thus providing an environment like natural tissues (Zu et al., 2022). Moreover, drug-loaded hydrogels are easily fine-tuned by varying parameters such as crosslinking degree, varying the polymer concentration and molecular weight, and mixing with other polymers and/or bioactive molecules (Thang et al., 2023). Thus, allowing the optimization of drug delivery strategies, both from a general and a personalized point-of-view. Despite these advantages, the extrusion-based printing of hydrogels remains challenging. For example, the evaporation of water or solvents during and after printing can cause undesirable shrinkage and further deformation, altering the physical dimensions and mechanical properties of the final product. Additionally, the high water content of hydrogel-based formulations can cause them to easily spread or deform, resulting in poor printing accuracy. This excessive water content also compromises the mechanical stability of the printed objects, leading to a lack of structural integrity and making them prone to collapse or deformation under minimal stress. In contrast, formulations with low water content are too hard to extrude, resulting in under extrusion and poor printing accuracy (Bom et al., 2022).

One characterization technique that has often linked the printing accuracy and shape fidelity of materials to their "printability" in SSE is rheology (Temirel et al., 2022). Rheology is a tool used to describe the flow behaviour of materials, it is of immense importance within the extrusion-based 3D printing of hydrogels to describe the comportment of the material before, during, and after printing (Bercea, 2023). For example, the viscosity of the material and its shear thinning properties will determine how easily it can flow through the nozzle (during printing), and its ability to maintain its shape after being extruded (after printing) (Bercea, 2023; Liu et al., 2019). However, the data collected from rheological analysis can be not only time-consuming but also overwhelming for inexperienced users. These individuals are presented with various rheological measurements, ranging from traditional viscosity assessments to more advanced studies such as oscillatory amplitude shear analyses. With this abundance of observations, discerning patterns becomes increasingly challenging and often demands years of experience (Elbadawi et al., 2020).

In our prior study (Aina et al., 2024), we tackled the challenges associated with rheological analyses by conducting oscillatory and rotational measurements, intending to facilitate the rheological characterization of materials. Our results indicated that out of the 11 parameters obtained, the phase angle (δ) could potentially suffice as an adequate metric for evaluating printability, Pr. We observed that overgelled formulations that were difficult to extrude (Pr > 1.14) had δ values lower than 6°. Whereas formulations with δ between 10° and 14° resulted in optimal printability ($0.94 < Pr < 1.14$). However, pastes with δ above 14° also displayed optimal Pr due to their high elastic modulus or high yield stress. Conversely, undergelled samples with high δ but low elastic modulus or yield stress exhibited $Pr < 0.94$, necessitating post-treatment to achieve mechanically stable objects. Therefore, while δ provided a good estimate of the printability of samples, we recommended that either the elastic modulus or yield stress be used as a complement to evaluate the sample's mechanical strength. Other studies have also highlighted the use of one rheological parameter to evaluate printability. For example, Ribeiro et al. (2017) proposed a model using yield stress to predict filament deformation and Liu et al. (2019), highlighted that the shear-thinning behaviour of a material was related to its extrudability. What remained consistent across these studies, however, was the observation that a single rheological parameter alone could not comprehensively elucidate printing outcomes. Nonetheless, certain parameters displayed notable correlations with specific printing outcomes. Despite this, rheological evaluation remains insufficient in predicting the true printing performance of hydrogel-based formulations (Falcone et al., 2024; Müller et al., 2020). Moreover, there is a notable absence of alternative and simpler characterization techniques for evaluating the printability of these formulations.

Another technique commonly used to characterize hydrogel samples is texture profile analysis (TPA) (Kim et al., 2017; Le Tohic et al., 2018; Theagarajan et al., 2020; Matas et al., 2023; Ganatra et al., 2024; Rodríguez-Herrera et al., 2024). TPA is widely employed across various industries to quantify physical properties by measuring the force required to compress or stretch a sample with a probe. The functionality of a texture analyser varies depending on the selected probe or fixture, enabling a range of tests including compression, extension, cutting, bending, and shearing to assess properties such as fracturability, chewiness, stickiness, and consistency (Nishinari and Fang, 2018). While TPA provides valuable information on both textural (sensory) and mechanical properties of samples, its primary application is often related to textural characteristics (Carranza et al., 2023; Ren et al., 2023). In addition, TPA parameters do not directly correlate with rheological properties, limiting their scope of application (Jones et al., 2002). Therefore, sample characterization often requires the use of both a rheometer and a texturometer. Although efforts have been made to address this issue, for instance, Gilbert et al. (2013) observed significant correlations between textural parameters and rheological parameters related to viscosity or stress, while Jones et al. (2002) employed dimensional analysis to define textural parameters using rheological terms. Notably, the analytical model of Zhou et al. (2013) was used to derive the yield stress, flow, and consistency index of carbopol-based 3D printing pastes (Zidan et al., 2019). However, there have been no reports of obtaining rheological information by considering the texturometer, particularly one equipped with a syringe, as a capillary rheometer. Moreover, some of these studies have relied on complex models dependent on multiple variables that may be time-consuming and require training needs.

Furthermore, as SSE typically involves extruding material through a constricted nozzle, capillary rheology experiments are more adapted to the measurement of the sample's shear viscosity and shear-thinning properties at high shear rate regime. The interest in a high shear rate regime lies in the extrusion process happening at a faster time scale than what most rotational rheometers are capable of measuring. Thus, the use of a texturometer as a capillary rheometer not only provides rheological data that is more related to the extrusion process, but also makes it possible to obtain textural, mechanical and rheological data using the same equipment, reducing training requirements. We therefore described, in this study, a process in which a texturometer fitted with a syringe (a capillary rheometer) was used to obtain shear viscosity data. Furthermore, the parameters from fitting the data to a power law equation as well as the flow curve were compared to those obtained from a rotational rheometer in the study by Aina et al. (2024). The identification of a relationship between these two techniques would enable the use of a texturometer as a method by which the rheological properties of gel systems may be routinely examined.

2. Material & method

2.1. Material

Agar (A), anhydrous caffeine (C) and pulverized sucrose (S) were purchased from Cooper's Laboratory, France. Hydroxypropyl methylcellulose (HPMC, H) (USP 2208 grade, 4000 cp, Controlled release (CR) Premium, MW = 2.1×10^5 g/mol, 8.1% hydroxypropyl and 22% methoxy substituted) was obtained as a gift from Colorcon Ltd, France. The samples were prepared with deionized water obtained with Aquadem® water demineralizer (Veolia Waters Technology, France).

Table 1
Sample notation and aqueous composition (in % w/w).

Notation	Agar (A)	HPMC (H)	Sucrose (S)	Caffeine (C)
3A	3	–	–	–
3A2H	3	2	–	–
3A3H	3	3	–	–
3A4H	3	4	–	–
3A5H	3	5	–	–
4A	4	–	–	–
4A2H	4	2	–	–
4A3H	4	3	–	–
4A4H	4	4	–	–
4A5H	4	5	–	–
10S0C	3	2	10	0
10S1C	3	2	10	1
10S2C	3	2	10	2
10S3C	3	2	10	3
10S5C	3	2	10	5
10S7C	3	2	10	7
10S10C	3	2	10	10

2.2. Preparation of hydrogels

Hydrogels were prepared like our previous study (Aina et al., 2024). Briefly, the samples: A, H, S and C were dissolved in deionized water in the proportions (in % w/w) as shown in Table 1. The weighed powders were placed in a beaker, after which, they were mixed to ensure powder homogenization using a stainless-steel laboratory spatula. While stirring, deionized water heated to 98 °C was slowly added to the homogenized powder mixture. Upon forming a lump-free paste, the beaker was placed in a water bath at 95 °C until an amber or white-coloured solution was formed. This solution was then left at room temperature (20 °C) overnight before rheological and printability assessment was conducted.

2.3. Rheological analysis

The rheological behaviour of the formed gels/pastes was investigated using a RheoStress RS 600 Rheometer (Themo Scientific HAAKE, France). Plate–plate geometry (diameter = 35 mm) was used at a gap height between 0.1 and 0.5 mm, set based on the sample being analysed. All measurements were performed in duplicates and conducted at 20 °C. Flow curves were obtained through rotational tests in which the shear rate was reduced stepwise from 10–10^{-2} s^{-1} on a logarithmic scale with 10 s per data point. The samples were also pre-sheared at 10 s^{-1} for 30 s and equilibrated for 30 s before all measurements were taken.

2.4. Capillary extrusion rheometer

The force applied to the syringe plunger to extrude the samples was measured using a TX-700 texture analyser (Lamy Rheology ™, France) fitted with a syringe actuator (TX-SAF) as shown in Fig. 1(a). Briefly, each sample was prepared as mentioned above (Table 1) and was loaded into the syringe (radius of orifice, r_s and length, l_s of tip were 0.885 and 10 mm, respectively) using a spatula and the probe was moved downwards until in contact with the plunger of the syringe (at the 5 mL volume mark). All samples were pre-sheared by extruding out of the syringe before the analysis was performed.

Thereafter, the syringe piston (radius, R_s of piston = 8 mm) was moved to a displacement of 10 mm at a displacement speed (v) of 0.05, 0.5, 1, 5 and 10 mm/s and the corresponding force–displacement curve was obtained. The volumetric flow rate (Q) during the displacement was determined according to Eq. (1).

$$Q = \pi R_s^2 v \tag{1}$$

Fig. 1(b) shows a pattern diagram of the force acting on the syringe during the extrusion of the sample. The total force measured by the rheometer, F_t was defined as the sum of the hydrodynamic force, F_h and the dynamic frictional force, F_f (Kasem et al., 2019). F_f was obtained by measuring the force required to push an empty syringe. The hydrodynamic force, which depended on the sample's viscosity, was thus the difference between the measured force and the frictional force. The pressure drop within the capillary (excluding the entrance pressure drop), caused by the viscosity of the sample, was subsequently determined using the formula provided in Eq. (2).

$$\Delta P = \frac{F_h}{\pi R_s^2} = \frac{F_t - F_f}{\pi R_s^2} \tag{2}$$

A derivation of the Hagen–Poiseuille equation gives the apparent shear rate, $\dot{\gamma}_a$ (s^{-1}), apparent shear stress, τ_a (Pa), and apparent shear viscosity, η_a (Pa s) of a Newtonian fluid flowing through the tip of the syringe, as shown in Eqs. (3) to (5).

$$\dot{\gamma}_a = \frac{4Q}{\pi r_s^3} \tag{3}$$

$$\tau_a = \frac{r_s \Delta P}{2 l_s} \tag{4}$$

$$\eta_a = \frac{\tau_a}{\dot{\gamma}_a} \tag{5}$$

2.5. Data modelling

Due to the limited sensitivity of both capillary and rotational rheometers at extremely lower shear rates, as well as the limited robustness of rotational rheometers at high shear rates, it becomes challenging to acquire the complete flow curve of samples using either method alone, or even when both methods are combined (Luo et al., 2021; Herrada-Manchón et al., 2023). However, a model suitable for the intermediate shear rate regime (0.1–10^4 s^{-1}) and applicable within the operating range of both techniques is the Ostwald-de Waele, or power-law model (Lakkanna et al., 2016). This model, Eq. (6), corresponds to the linear portion of the flow curve to which it can be effectively applied.

$$\eta = K \dot{\gamma}^{n-1} \tag{6}$$

where η is the viscosity (Pa s), K is the consistency index (Pa s^n), $\dot{\gamma}$ is the shear rate (s^{-1}) and n is the flow behaviour index (dimensionless).

For Newtonian fluid there is a linear relationship between shear rate and shear stress ($n = 1$), whereas, for non-Newtonian fluids, the relationship is nonlinear ($n \neq 1$). Moreover, Newtonian fluids maintain a constant viscosity regardless of the shear rate, whereas the viscosity of non-Newtonian fluids vary in response to the shear rate. Non-Newtonian fluids that exhibit an increase in viscosity with shear rate are termed shear-thickening or dilatant fluids ($n > 1$), while those that demonstrate a decrease in viscosity as the shear rate increases are known as shear-thinning or pseudoplastic fluids ($n < 1$) (Herrada-Manchón et al., 2023; Ansari et al., 2020).

2.6. Printability analysis

Square grids were printed using a pneumatic 3D Printer (Delta WASP 2040, Italy) fitted with an 0.8 mm nozzle diameter. The layer height and the printing speed used were 0.4 mm and 20 mm/s, respectively. Depending on the extrusion of continuous lines, the pressure was maintained between 4 to 5 bar (highest pressure was for 10S10C). Images of 4.6 mm x 4.6 mm printed squares (5 replicates) were analysed in ImageJ to determine their perimeter, L, and area, A. Pr was subsequently calculated using the following equation:

$$Pr = \frac{L^2}{16A} \tag{7}$$

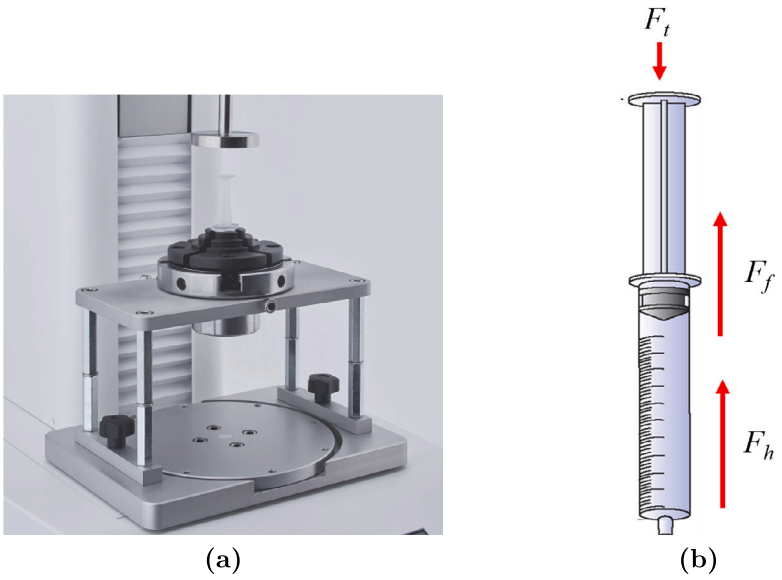

Fig. 1. LAMY TX 700 rheometer fitted with syringe actuator (a) Schema representing the forces acting on the syringe (b).

2.7. Data analysis

Principal component analysis (PCA) was used to identify clusters of the sample's flow behaviour based on their printability. The K and n obtained from the capillary and rotational rheometer (K_{cap}, n_{cap}, K_{rot} and n_{rot}, respectively) were first mean-centred and scaled to the variance. The matrix was then decomposed into principal components (PCs) by applying singular vector decomposition (SVD). The visualization was conducted by plotting the factor loadings matrix and displaying the scores of components with eigenvalues exceeding 1. This was achieved using the biplot function available in MATLAB's Statistics Toolbox. Non-linear predictive models were also built with the rheological parameters obtained using the different rheological measurement techniques. The predictive performance was evaluated using the regression coefficient (R^2Y) from the model and the actual 3D printing data. An R^2Y value between 0.66–0.81 indicates that the model can be used for screening, values between 0.83–0.90 indicate that the model is usable with caution for most applications, whereas values between 0.92–0.96 indicate that the model is usable in quality assurance (Onsawai et al., 2021).

2.8. Statistical analyses

Data analyses were performed using MATLAB R2023a (MathWorks, USA). A two-sample t-test, utilizing the student's t-test method, was employed to compare the mean values. All analyses were conducted with statistical significance set at $p \leq 0.05$.

3. Results and discussion

3.1. Determination of dynamic frictional force

The protocol described in Section 2.4 generates the data used to plot the force–displacement curves of all samples. This curve, as shown in Fig. 2, typically consists of three sections: an initial gradient, as the plunger overcomes friction from the barrel, a force maximum, and a plateau, as the material is extruded at a steady state (Robinson et al., 2020). In the context of syringes or similar piston-driven devices, the forces required to initiate and maintain movement of the piston when there is no fluid present inside the syringe is referred to using the terms empty break-loose force and gliding force, respectively (Prasetyono and Adhistana, 2019). The empty break-loose force is the initial force needed to overcome static friction between the piston and the syringe barrel — it initiates movement from a stationary position. Gliding force, on the other hand, maintains the piston's movement once initiated and includes the dynamic friction (Pstras, 2016; Lorenz et al., 2013). The dynamic/kinetic frictional force is encountered when two surfaces are in relative motion, representing the resistance to flow, and is thus more relevant for the calculation of viscosity. The force–displacement diagram of an empty syringe at different displacement speeds is presented in Fig. 2(a). The gliding force at lower displacement speeds (0.05, 0.5 and 1 mm/s) was considered either too high or too low and therefore was not utilized. However, at 5 and 10 mm/s, the empty break-loose and gliding force seemed more appropriate and corresponded to the forces recorded by Loosli et al. (2018). Ultimately, we chose to determine the frictional force, F_f at 10 mm/s. The measurement across ten (10) experiments is presented in Fig. 2(b) and was estimated as 2.53 ± 0.09 N.

3.2. Determination of the extrusion force

The force–displacement curve of some selected samples is shown in Fig. 3. Unlike the rest, samples containing only agar (e.g. 3A and 4A) showed noisy peaks at the plateau region, which could be attributed to particle occlusion and/or air bubble outgassing. This noisiness could also be due to the samples being inhomogeneous and/or highly fracturable. Samples with this type of behaviour usually show poor printability (Matas et al., 2023) and in our previous work (Aina et al., 2024), they were classified as being overgelled. Nevertheless, we took an average of the force of all samples at the plateau region (designated between a displacement of 4.44 and 7.88 mm) as an estimation of the total force, F_t needed to extrude the sample.

Generally, F_t increased with the increase of the displacement speed and the viscosity of the sample. At each displacement speed, the highest F_t recorded were those of the 10S10C sample. It should however also be noted that, the plateau force in terms of texture profile analysis, refers to the hardness of the sample and the greater the hardness, the more difficult the extrusion (printing). However, with the printer used, we were able to achieve the printing of 10S10C (intermediate printability, $0.94 < Pr < 1.14$) due to the extrusion pressure being within the range of the sample's requirement as well as the pre-shearing that was performed at the nozzle and before deposition.

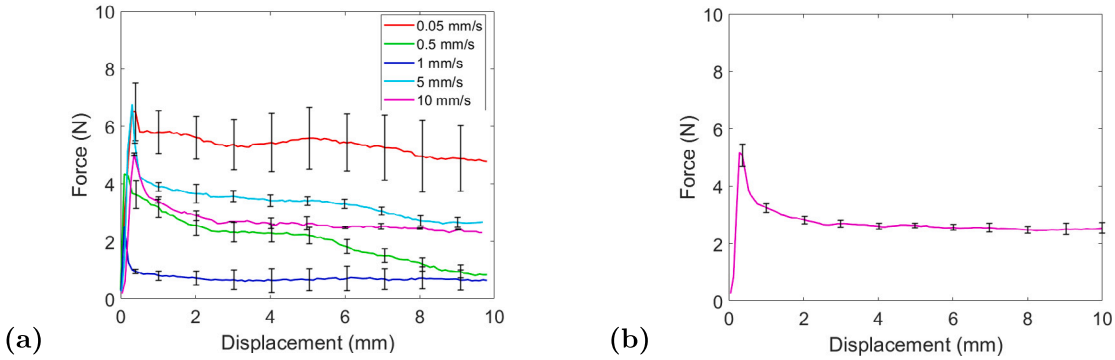

Fig. 2. Force–displacement curve of an empty syringe, F_f at different displacement speeds (a) and at 10 mm/s (b). Datapoint is mean of 3 and 10 measurements with 10 error bars of the standard deviation for (a) and (b), respectively.

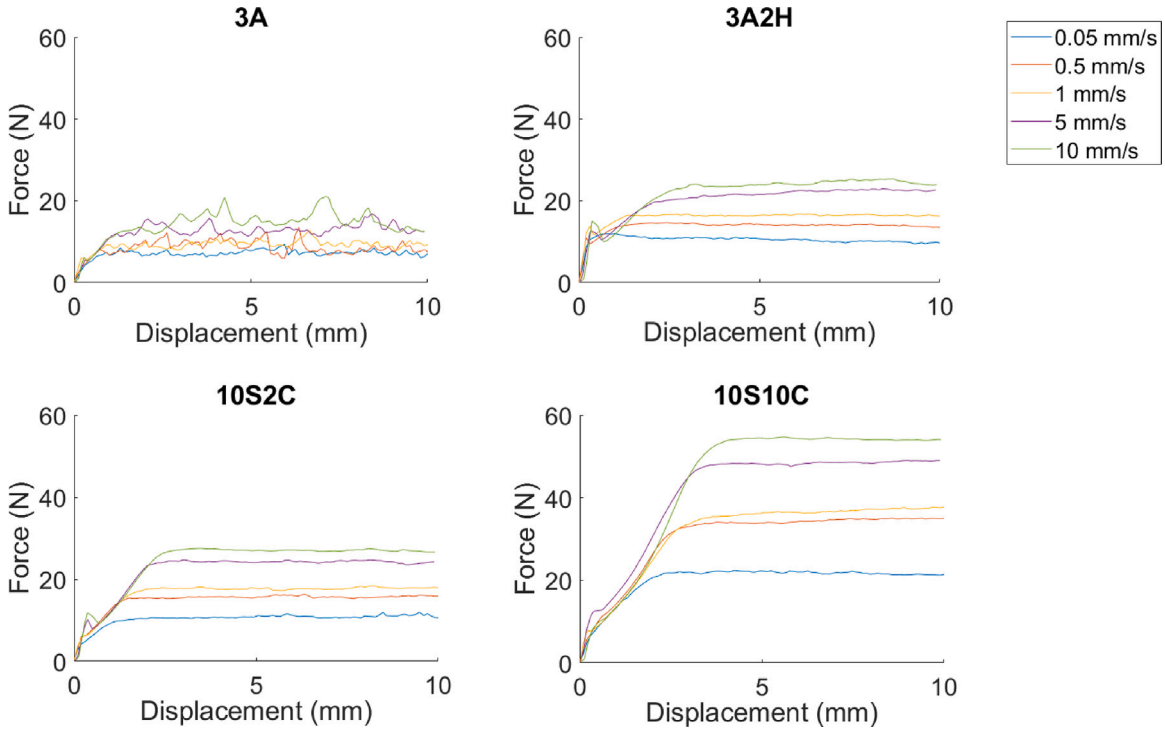

Fig. 3. Force–displacement curve of some selected samples at different displacement speeds.

3.3. Calculation of the rheological parameters

The shear flow of a sample through a capillary die (here, the syringe's orifice) has been well characterized and the Hagen–Poiseuille equation may be used to calculate its shear rate, and viscosity as illustrated in Section 2.4. However, the equations used in capillary rheology assume that the flow is fully developed, steady, isothermal, and laminar. Additionally, it is assumed that the fluid is incompressible, and the effects of gravity and inertia can be disregarded (Lewandowski et al., 2022; Osswald and Rudolph, 2014). To accurately determine the viscosity, additional factors need consideration. These include the pseudoplastic properties of the gels and deviations from ideal flow assumptions, as outlined in the Poiseuille equation (Lewandowski et al., 2022).

An example of such correction is the Bagley correction which accounts for losses measured due to inlet and outlet effects, and non-fully developed flow conditions, particularly in viscoelastic fluids (Calafel et al., 2020). However, in the case of gels, their rheological behaviour is often significantly different from those of traditional viscoelastic fluids. At low shear rates, gels often display solid-like behaviour and have high resistance to flow (Malkin et al., 2023). This means that they resist deformation and flow relatively slowly when subjected to minimal shear forces. In contrast, at high shear rates, gels may undergo shear-thinning behaviour, where their viscosity decreases as the shear rate increases. While the resistance to flow may be reduced compared to low shear rates, gels still maintain some degree of resistance and do not behave purely as liquids. Due to this behaviour, gels often flow more uniformly through the capillary, resembling a more ideal flow condition compared to other polymers. Consequently, the Bagley correction was neglected in this study.

Based on the assumption that sample flow during analysis occurs within the yielded region, where wall stress equals the apparent stress, it became necessary to determine the wall shear rate, especially for non-Newtonian materials. In such materials, the plug flow through the centre of a pipe is only surmountable at the pipe walls (Ihmoudah et al., 2023). Additionally, the distribution of flow across the material results in a higher shear rate at the wall compared to their Newtonian counterparts. To address this, the Rabinowitsch equation, as illustrated in Eqs. (8) and (9), was employed to correct the obtained data (Gooch,

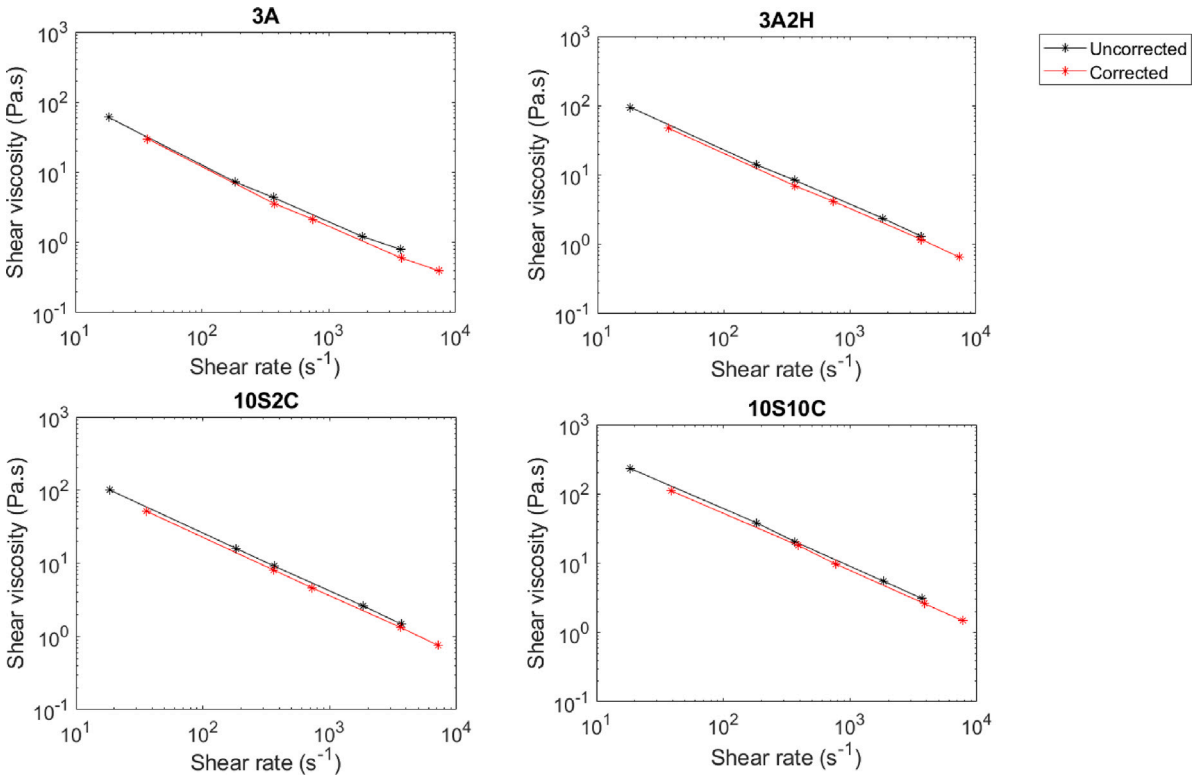

Fig. 4. Comparison of the uncorrected rheological data and data obtained after Rabinowitsch correction using the capillary rheometer (via texturometer).

2007; Osswald and Rudolph, 2014). This correction effectively increases the corrected shear rates ($\dot{\gamma}_c$) and decreases the corrected shear viscosity (η_c), since n is less than 1, resulting in a downward shift of the curve to the right, as depicted in Fig. 4.

$$\dot{\gamma}_c = \left[3 + \frac{d(lnQ)}{d(ln\tau_a)}\right] \frac{\dot{\gamma}_a}{4} \tag{8}$$

$$\eta_c = \frac{\tau_a}{\dot{\gamma}_c} \tag{9}$$

Furthermore, while the syringe diameter used to generate the force–displacement curve was larger than that of the 3D printer nozzle, smaller syringe diameters primarily affected the shear rate and corresponding viscosity, also shifting the curve downward and to the right. Consequently, smaller diameter syringes can be used to induce higher shear rates on the sample while measuring the viscosity at these rates. In this study, we achieved a shear rate range of 10 to 10^4 s^{-1}, which we considered well within the range of the 3D printer used (Aina et al., 2023).

3.4. Flow behaviour

The flow curve of selected samples is depicted in Fig. 5. It is noteworthy that the power law model demonstrated a strong fit for the data obtained from both techniques (R^2 >0.9). Notably, the rotational rheometer provided data within a lower shear rate range (10–10^{-2} s^{-1}), whereas the capillary rheometer yielded data within a higher shear rate range (30–9000 s^{-1}). However, the shear rate range of the capillary rheometer was determined only after completing all calculations. This approach was necessary due to the dependency on multiple variables, particularly the shear-thinning properties of the sample. As a result, a minimum of three data points was necessary to ascertain the required corrections before establishing the assessed shear rate range by the capillary rheometer. While this process may present a challenge, we have provided a Python script in the data availability statement. This script performs the calculations using a similar setup, making it easier for users to obtain the shear viscosity data as well as the power-law fit of the data. In addition, it is noteworthy that the data obtained from the capillary rheometer (via the texturometer) exhibited strong correlations with those obtained from the rotational rheometer. Consequently, this allowed for the comprehensive characterization of the gels across a broader range of shear rates, despite the initial limitations posed by the capillary rheometer's assessment method. Moreover, the shear rate range of 3D printers is likely to fall within the higher shear rate regime of a capillary rheometer.

Furthermore, since the viscosity of pseudoplastics decreases as the shear rate increases, they are better extruded when subjected to external forces, thus making them preferable for 3D printing applications. These materials also demonstrate a certain level of inherent stability, enabling them to retain the printed shape or pattern even after the external driving force is removed. Conversely, shear-thickening fluids are not recommended, as they gradually return to a state of easy flow when at rest (Barrulas and Corvo, 2023). Therefore, the lower the value of n, the better the shear thinning properties which generally means the better the extrudability and the shape retention of the material. In addition, while low viscous materials (low K) can be easily extruded, materials whose viscosity is too low are generally unsuitable for SSE, since the final objects may collapse after printing. On the other hand, highly viscous materials (high K) may not flow and are usually associated with the requirement of high mechanical force and/or in-homogeneous flow.

From our prior investigation using a rotational rheometer (Aina et al., 2024), we found that all samples demonstrated shear-thinning behaviour (n <1), this was also true in this study. However, the response to variations in agar, HPMC, and caffeine contents differed from our previous findings. Specifically, in this study, we noted a decrease in n with agar concentration, no clear trend in the behaviour of n concerning HPMC concentration, and consistent values of n across samples containing caffeine. On the other hand, the behaviour of K in response to variations in agar, HPMC, and caffeine contents mirrored our previous findings, except the decrease observed between 10S0C

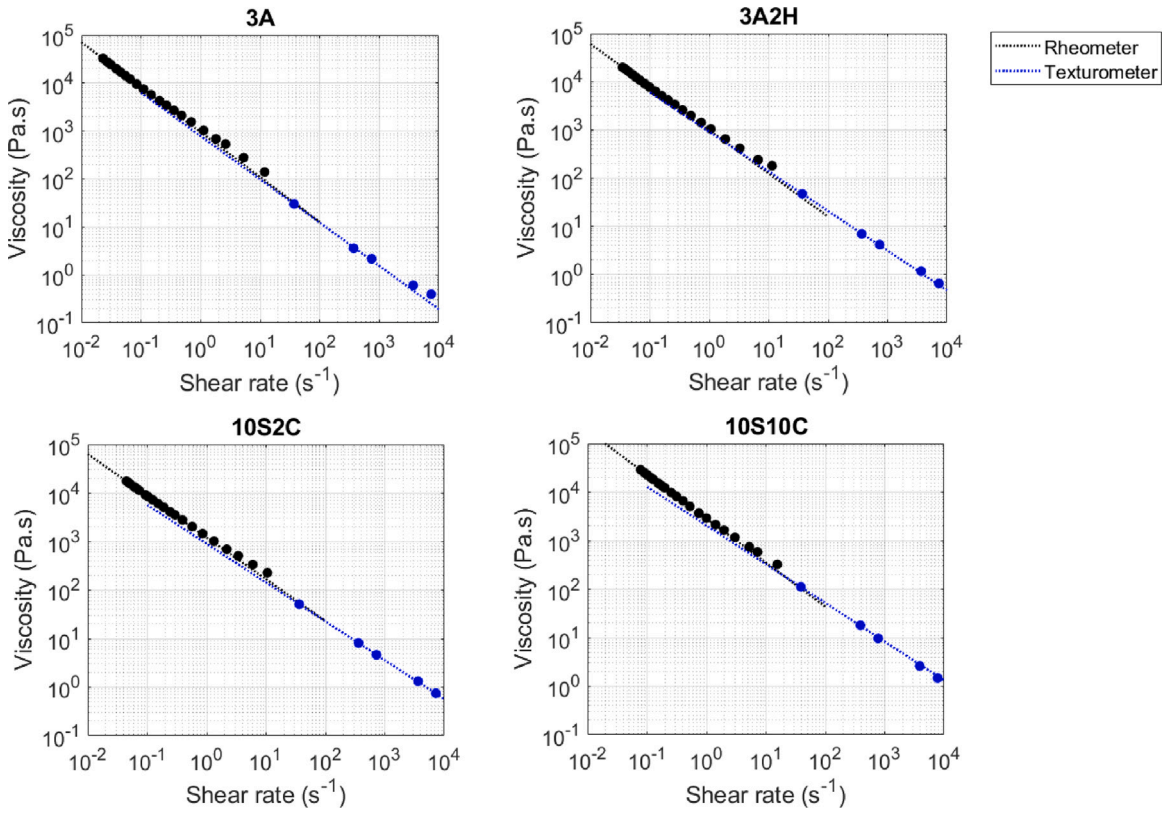

Fig. 5. Curve fitting to power law model of the rheological data and data obtained from the capillary rheometer (via a texturometer).

and 10S2C (Figs. 6(c) and 6(d)). Notably, samples containing 4A and 10S10C exhibited high K values, consistent with our earlier study where the former displayed non-uniform flow during extrusion and the latter required greater mechanical force for extrusion.

It should also be noted that similar conclusions obtained from K could be drawn from the analysis of force–displacement diagrams (Fig. 3). Hence, it is unsurprising that some researchers prefer to assess printability based on force–displacement diagrams (Matas et al., 2022; Varela et al., 2023; Venkatachalam et al., 2023). In addition, rotational measurements may not be necessary for samples that exhibit clear non-uniform flow patterns (3A and 4A) or those that require extrusion forces beyond the operational limits of the 3D printer (10S10C, although it remained printable in our case). The use of a texturometer to obtain rheological data thus holds the potential to streamline the typically time-consuming process associated with rheological characterizations.

3.5. Comparison of both techniques

Although the mean value of the parameters obtained from the flow curve of the rotational rheometer showed lower n and higher K compared to the capillary rheometer (Figs. 7(a) and 7(b), respectively), this difference occurs because the power law model characterizes the material's flow within the shear rate range to which the parameters K and n are fitted (Chhabra, 2010; Ansari et al., 2020; Bercea, 2023). Therefore, this difference is linked to the flow behaviour during low (rotational rheometer) or high (capillary rheometer) shear rate regimes. Furthermore, the results of an independent-samples t-test carried out to compare the mean values of K_{cap} (samples = 17, Mean = 1444.39 Pa s^n, SD = 616.49 Pa s^n) and K_{rot} (samples = 17, Mean = 1607.62 Pa s^n, SD = 609.69 Pa s^n) as well as the mean values of n_{cap} (samples = 17, Mean = 0.18 (–), SD = 0.05 (–)) and n_{rot} (samples = 17, Mean = 0.16 (–), SD = 0.07 (–)), revealed no significant difference between the mean values of the two techniques for either parameter ($p = 0.41$). This suggests that, despite any observed variability in the measurements, there is insufficient evidence to conclude that the means obtained from capillary rheometer are significantly different from those obtained from the rotational rheometer. In addition, when the data obtained from both the rotational and capillary rheometer were used together to fit the power law model, the mean values of the parameters obtained were practically the same ($p = 1.00$) as those of the rotational rheometer (Fig. 7). Thereby showing a continuity of data from the rotational rheometer by the data obtained from the capillary rheometer and the application of the texturometer as a capillary rheometer to obtain rheological information.

3.6. Evaluation of printability

Printability was previously evaluated in our study (Aina et al., 2024). Here, we aim to emphasize the role of each excipient used and the rationale behind the different mixtures. Agar was used as the principal gelling agent due to its ability to form a firm yet flexible gel at low concentrations upon cooling. However, its high gel strength makes it difficult to extrude at low temperatures, resulting in the deposition of twisted strings. Additionally, when printed alone agar-based formulations resulted in objects with low printing resolution and a coarse appearance (Aina et al., 2023). This was highlighted by the Pr of agar-based gels (3A and 4A), both being greater than 1.14. In contrast, HPMC dissolves to form a solution when cooled (Khater et al., 2023; Ramli et al., 2023). Using this property, HPMC was added to the formulation to reduce the dense network of agar gels and promote the formation of uniform and smooth printing filaments. Formulations with excess HPMC were, however, less firm and collapsed after printing (Pr <0.94) due to poor shape retention. However, formulations containing 2% and 3% HPMC had better shape retention, due to the contribution of agar, and good extrudability, due to HPMC. These formulations had Pr values between 0.94 and 1.14, making them ideal candidates for printing.

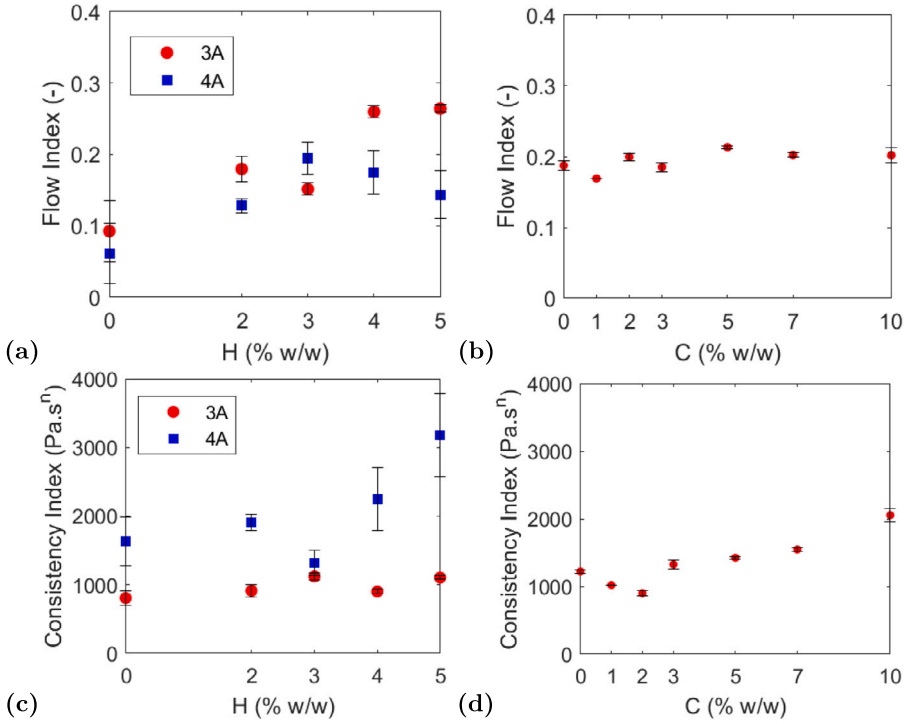

Fig. 6. Results of A and AH gels of different HPMC concentrations and 10S of different caffeine concentrations based on their flow (a & b, respectively) and consistency index (c & d, respectively).
Error bars are standard deviations based on duplicate experiments.

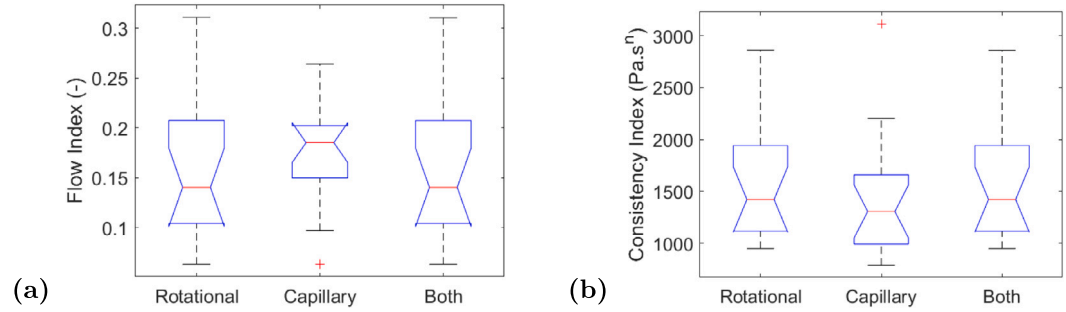

Fig. 7. Boxplot representation of the total mean values of flow (a) and consistency index (b) obtained from the rotational, capillary (via texturometer) and data using both techniques.

3.7. Data visualization using PCA biplot

The biplot representation of the rheological parameters is presented Fig. 8. There was a clear separation of the samples based on their printability, finding similar to Aina et al. (2024). Principal Component 1 (PC 1) described parameters related to the mechanical strength of the formulation to hold the printed structures and the magnitude of force necessary to extrude samples. PC 1 accounted for 50.4% of the total sample variance, with the consistency indexes: K_{cap} and K_{rot} positively correlating with this axis. Regarding this PC, samples that had higher values of K (e.g. 4A5H) required higher extrusion force (or pressure) to print and were at the top, whereas samples (e.g. 3A) with lower values of K, required lower extrusion force and were at the bottom. Principal Component 2 (PC 2) corresponded to 37.2% of the total variance, n_{cap} and n_{rot} correlated positively with this axis. Ductile samples (e.g. 3A5H) had higher n and were at the left whereas, brittle samples (e.g. 4A) had lower n and were at the right. Lastly, principal component 3 (PC 3) corresponded to 11.6% of the explained variance. n_{cap} showed a negative correlation with this axis, whereas n_{rot} displayed a positive correlation. At low shear rates, n_{rot} is related to the force required to initiate flow whereas at high shear rates, n_{cap} is related to the force required to sustain flow. Furthermore, these forces, required to initiate and sustain flow, are referred to as the yield and flow stresses, respectively. They both have been correlated with enhanced mechanical strength to support extruded layers (Herrada-Manchón et al., 2023; Zhu et al., 2019). Therefore, PC 1 was attributed to the extrusion force necessary to extrude the gels, PC 2 the sample's ductility and PC 3 the shape retention ability of the extruded samples, a finding consistent with our previous study (Aina et al., 2024). Thus, suggesting that these parameters convey similar information regardless of the measurement technique.

3.8. Data modelling

The non-linear regression coefficients of the modelling of the rheological parameters obtained from the two techniques are presented in Table 2. Evaluating the impact of K and n on the regression coefficient revealed that n had a greater influence on the estimation of printability. This is likely due to the definition of printability: brittle samples had higher Pr while those that were ductile had lower values. Consequently, Pr would be more correlated with n than with K. Specifically,

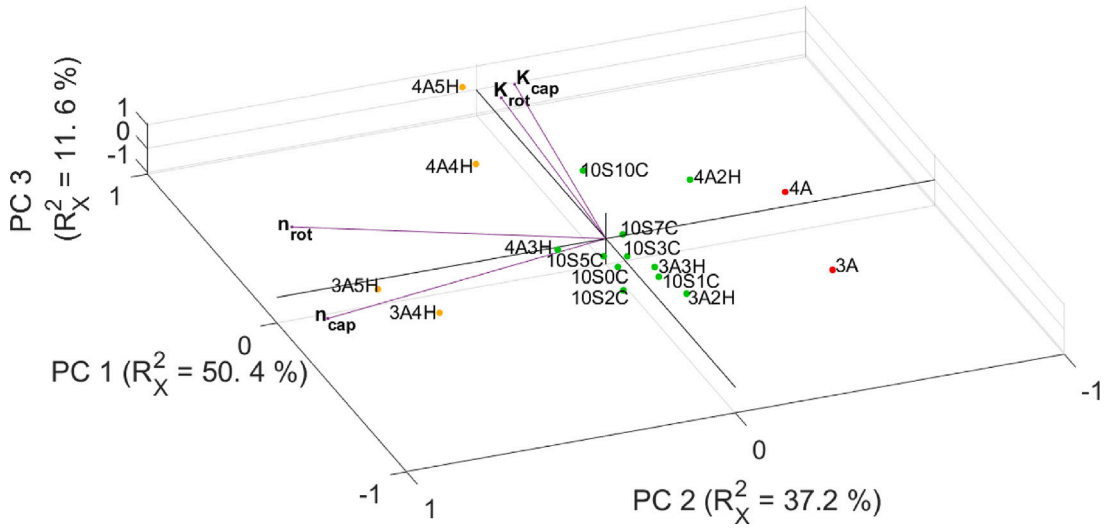

Fig. 8. PCA score and loading plot. Coloured markers were based on the printability of the formulations: red: $Pr > 1.14$, green: $0.94 < Pr < 1.14$ and yellow: $Pr < 0.94$.

Table 2
Prediction models for printability.

$K^p n^p$	Capillary (via texturometer)		Rotational	
	Prediction formula	R^2Y (%)	Prediction formula	R^2Y (%)
K^1n^1	$1.6399 - 0.0001 * K - 2.5437 * n$	82.62	$1.2933 - 0.0001 * K - 1.0482 * n$	37.07
K^1n^2	$2.3101 - 0.0003 * K - 10.051 * n + 0.0014 * K * n + 17.786 * n^2$	96.40	$1.920 - 0.0002 * K - 7.264 * n + 0.0009 * K * n + 12.661 * n^2$	59.15
K^2n^2	$2.391 - 0.0004 * K - 10.336 * n + 0.0016 * K * n + 17.786 * n^2$	96.62	$1.825 - 0.0001 * K - 7.653 * n + 0.0009 * K * n + 13.326 * n^2$	60.03

samples with higher n values, although they required more force to extrude, demonstrated good ductility compared to those with lower n, whereas the value of K had a similar effect on the extrusion force but related more to shape retention ability than to the ductility. Herein lies one of the shortcomings of this semi-quantitative method for assessing printability. Although samples with low Pr may be thought of as having good "printability", this is not necessarily true. Such samples only possess good ductility or extrudability. Nevertheless, evaluating the Pr of a sample is a much faster method, and samples with Pr that are too low (in this study, less than 0.94) can be avoided.

In addition, among the models assessed, K_{cap} and n_{cap} exhibited the highest R^2Y values when using a second-degree polynomial equation involving both K and n. Notably, the lower influence of K on Pr allowed for the simplification of the polynomial equation by eliminating the K^2 coefficient. Conversely, while K_{rot} and n_{rot} also displayed the highest R^2Y values in the second-degree polynomial of K and n, their R^2Y was found to be lower compared to that obtained from the capillary data. It can therefore be inferred that K_{cap} and n_{cap} performed better in estimating the Pr of the samples in this study than K_{rot} and n_{rot}. This superior performance may be attributed to the capillary rheometer's capability to measure the flow behaviour of the samples at higher shear rates, which closely resemble the conditions experienced during 3D printing. In a previous study (Aina et al., 2023), the shear rate during the printing process was calculated to be 200 s^{-1}. Therefore, the capillary rheometer, by operating at higher shear rates, may provide a more representative assessment of the rheological properties relevant to the 3D printing process.

4. Conclusion

In this study, we proposed the utilization of a texture analyser equipped with a syringe as a capillary rheometer to gather rheological data. Following the application of the Hagen–Poiseuille equation and Rabinowitsch correction for the computation of shear viscosity, the corrected data obtained from the capillary rheometer (via a texturometer) were fitted to the power-law model. Subsequently, the parameters obtained were compared to those derived from a rotational rheometer in a previous study. The results indicated no significant differences in the mean values of the two rheological techniques, allowing for the rheological characterization across a larger range of shear rates. Furthermore, using principal component analysis, three components were correlated to the extrudability, extrusion force and shape fidelity of the samples using the rheological parameters obtained. Moreover, there was a better fit of the rheological parameters obtained from the capillary rheometer to the printability of the samples. This enhanced performance can be attributed to the shear rate of the 3D printer falling within the operating range of the capillary rheometer. Consequently, this study underscores the potential of employing a texture analyser for rheological data collection, addressing a longstanding challenge associated with textural profile analysis—specifically, the historical difficulty in acquiring rheological data. Additionally, the findings of this research suggest that capillary rheological data are better suited for assessing the printability of formulations for SSE 3D printing.

Funding

The authors are grateful to the Occitanie Region and ANR "Investissements d'Avenir" program, ANR-18-EURE-0021 project, for funding.

CRediT authorship contribution statement

Morenikeji Aina: Writing – review & editing, Writing – original draft, Methodology, Investigation, Formal analysis, Data curation. **Fabien Baillon:** Writing – review & editing, Visualization, Software. **Romain Sescousse:** Writing – review & editing, Validation, Supervision. **Noelia M. Sanchez-Ballester:** Project administration, Investigation.

Sylvie Begu: Supervision, Project administration. **Ian Soulairol:** Validation, Supervision, Methodology, Investigation, Conceptualization. **Martial Sauceau:** Writing – review & editing, Validation, Supervision, Resources, Methodology, Funding acquisition, Conceptualization.

Declaration of competing interest

The authors declare the following financial interests/personal relationships which may be considered as potential competing interests: Martial Sauceau reports financial support was provided by French National Research Agency. Martial Sauceau reports financial support was provided by Occitanie Region. If there are other authors, they declare that they have no known competing financial interests or personal relationships that could have appeared to influence the work reported in this paper.

Data availability

A Python code that can be used to generate the shear viscosity data as well as calculate the rheological parameters is available here: pythonanywhere.com. Otherwise, the data that support the findings of this study are available from the corresponding author, MA upon request.

References

Aina, M., Baillon, F., Sescousse, R., Sanchez–Ballester, N.M., Begu, S., Soulairol, I., Sauceau, M., 2023. Characterization of the extrudability of hydrogel-based materials for 3D printing of heat-sensitive drugs. MATEC Web Conf. 379, 06002. http://dx.doi.org/10.1051/matecconf/202337906002.

Aina, M., Baillon, F., Sescousse, R., Sanchez-ballester, N.M., Begu, S., Soulairol, I., Sauceau, M., 2024. Evaluation of the printability of agar and hydroxypropyl methylcellulose gels as gummy formulations: Insights from rheological properties. Int. J. Pharm. 654, 123937. http://dx.doi.org/10.1016/j.ijpharm.2024.123937.

Ansari, S., Rashid, M.A.I., Waghmare, P.R., Nobes, D.S., 2020. Measurement of the flow behavior index of Newtonian and shear-thinning fluids via analysis of the flow velocity characteristics in a mini-channel. SN Appl. Sci. 2 (11), 1787. http://dx.doi.org/10.1007/s42452-020-03561-w.

Barrulas, R.V., Corvo, M.C., 2023. Rheology in product development: an insight into 3D printing of hydrogels and aerogels. Gels 9 (12), 986. http://dx.doi.org/10.3390/gels9120986.

Bercea, M., 2023. Rheology as a tool for fine-tuning the properties of printable bioinspired gels. Molecules 28 (6), 2766. http://dx.doi.org/10.3390/molecules28062766.

Bom, S., Ribeiro, R., Ribeiro, H.M., Santos, C., Marto, J., 2022. On the progress of hydrogel-based 3D printing: Correlating rheological properties with printing behaviour. Int. J. Pharm. 615, http://dx.doi.org/10.1016/j.ijpharm.2022.121506.

Calafel, I., Aguirresarobe, R.H., Peñas, M.I., Santamaria, A., Tierno, M., Conde, J.I., Pascual, B., 2020. Searching for rheological conditions for FFF 3D printing with PVC based flexible compounds. Materials 13 (1), 178. http://dx.doi.org/10.3390/ma13010178.

Carranza, T., Guerrero, P., de la Caba, K., Etxabide, A., 2023. Texture-modified soy protein foods: 3D printing design and red cabbage effect. Food Hydrocolloids 145, 109141. http://dx.doi.org/10.1016/j.foodhyd.2023.109141.

Chhabra, R.P., 2010. Non-Newtonian fluids: An Introduction. In: Krishnan, J.M., Deshpande, A.P., Kumar, P.B.S. (Eds.), Rheology of Complex Fluids. Springer, New York, NY, pp. 3–34. http://dx.doi.org/10.1007/978-1-4419-6494-6_1.

Cui, M., Pan, H., Su, Y., Fang, D., Qiao, S., Ding, P., Pan, W., 2021. Opportunities and challenges of three-dimensional printing technology in pharmaceutical formulation development. Acta Pharmaceut. Sinica B 11 (8), 2488–2504. http://dx.doi.org/10.1016/j.apsb.2021.03.015.

Elbadawi, M., Gustaffson, T., Gaisford, S., Basit, A.W., 2020. 3D printing tablets: Predicting printability and drug dissolution from rheological data. Int. J. Pharm. 590, 119868. http://dx.doi.org/10.1016/j.ijpharm.2020.119868.

Falcone, G., Schrüfer, S., Kuth, S., Mazzei, P., De Pasquale, S., Del Gaudio, P., Aquino, R.P., Boccaccini, A.R., Russo, P., 2024. Ready-to-print alginate inks: The effect of different divalent cations on physico-chemical properties of 3D printable alginate hydrogels. Carbohydrate Polymer Technol. Appl. 7, 100524. http://dx.doi.org/10.1016/j.carpta.2024.100524.

Ganatra, P., Jyothish, L., Mahankal, V., Sawant, T., Dandekar, P., Jain, R., 2024. Drug-loaded vegan gummies for personalized dosing of simethicone: A feasibility study of semi-solid extrusion-based 3D printing of pectin-based low-calorie drug gummies. Int. J. Pharm. 651, 123777. http://dx.doi.org/10.1016/j.ijpharm.2024.123777.

Gilbert, L., Picard, C., Savary, G., Grisel, M., 2013. Rheological and textural characterization of cosmetic emulsions containing natural and synthetic polymers: Relationships between both data. Colloids Surf. A 421, 150–163. http://dx.doi.org/10.1016/j.colsurfa.2013.01.003.

Gooch, J.W., 2007. Hagen–Poiseuille equation. In: Encyclopedic Dictionary of Polymers. Springer, New York, NY, p. 477. http://dx.doi.org/10.1007/978-0-387-30160-0_5664.

Herrada-Manchón, H., Fernández, M.A., Aguilar, E., 2023. Essential guide to hydrogel rheology in extrusion 3D printing: how to measure it and why it matters? Gels 9 (7), 517. http://dx.doi.org/10.3390/gels9070517.

Iftekar, S.F., Aabid, A., Amir, A., Baig, M., 2023. Advancements and limitations in 3D printing materials and technologies: a critical review. Polymers 15 (11), 2519. http://dx.doi.org/10.3390/polym15112519.

Ihmoudah, A., Abugharara, A., Rahman, M.A., Butt, S., 2023. Experimental and numerical analysis of the effect of rheological models on measurements of shear-thinning fluid flow in smooth pipes. Energies 16 (8), 3478. http://dx.doi.org/10.3390/en16083478.

Jones, D.S., Lawlor, M.S., David Woolfson, A., 2002. Examination of the flow rheological and textural properties of polymer gels composed of poly(methylvinylether-co-maleic anhydride) and poly(vinylpyrrolidone): Rheological and mathematical interpretation of textural parameters. J. Pharmaceut. Sci. 91 (9), 2090–2101. http://dx.doi.org/10.1002/jps.10195.

Kasem, H., Shriki, H., Ganon, L., Mizrahi, M., Abd-Rbo, K., Domb, A.J., 2019. Rubber plunger surface texturing for friction reduction in medical syringes. Friction 7 (4), 351–358. http://dx.doi.org/10.1007/s40544-018-0227-5.

Khater, E.-S., Bahnasawy, A., Gabal, B.A., Abbas, W., Morsy, O., 2023. Effect of adding nano-materials on the properties of hydroxypropyl methylcellulose (HPMC) edible films. Sci. Rep. 13 (1), 5063. http://dx.doi.org/10.1038/s41598-023-32218-y.

Kim, H.W., Bae, H., Park, H.J., 2017. Classification of the printability of selected food for 3D printing: Development of an assessment method using hydrocolloids as reference material. J. Food Eng. 215, 23–32. http://dx.doi.org/10.1016/j.jfoodeng.2017.07.017.

Lakkanna, M., Mohan Kumar, G., Kadoli, R., 2016. Computational design of mould sprue for injection moulding thermoplastics. J. Comput. Design Eng. 3 (1), 37–52. http://dx.doi.org/10.1016/j.jcde.2015.06.006.

Le Tohic, C., O'Sullivan, J.J., Drapala, K.P., Chartrin, V., Chan, T., Morrison, A.P., Kerry, J.P., Kelly, A.L., 2018. Effect of 3D printing on the structure and textural properties of processed cheese. J. Food Eng. vol. 220, 56–64. http://dx.doi.org/10.1016/j.jfoodeng.2017.02.003.

Lewandowski, K., Piszczek, K., Skórczewska, K., Mirowski, J., Zajchowski, S., Wilczewski, S., 2022. Rheological properties of wood polymer composites at high shear rates – Evaluation of additional pressure losses as a result of inlet effects. Composites A 154, 106804. http://dx.doi.org/10.1016/j.compositesa.2022.106804.

Liu, Z., Bhandari, B., Prakash, S., Mantihal, S., Zhang, M., 2019. Linking rheology and printability of a multicomponent gel system of carrageenan-xanthan-starch in extrusion based additive manufacturing. Food Hydrocolloids 87, 413–424. http://dx.doi.org/10.1016/j.foodhyd.2018.08.026.

Loosli, V., Germershaus, O., Steinberg, H., Dreher, S., Grauschopf, U., Funke, S., 2018. Methods To Determine the Silicone Oil Layer Thickness in Sprayed-On Siliconized Syringes. PDA J. Pharmaceut. Sci. Technol. 72 (3), 278–297. http://dx.doi.org/10.5731/pdajpst.2017.007997.

Lorenz, B., Krick, B.A., Rodriguez, N., Sawyer, W.G., Mangiagalli, P., Persson, B.N.J., 2013. Static or breakloose friction for lubricated contacts: The role of surface roughness and dewetting. J. Phys.: Condens. Matter. 25 (44), 445013. http://dx.doi.org/10.1088/0953-8984/25/44/445013.

Luo, S., Weinell, C.E., Okkels, F., Østergård, A.L., Kiil, S., 2021. On-line, non-Newtonian capillary rheometry for continuous and in-line coatings production. J. Coatings Technol. Res. 18 (3), 611–626. http://dx.doi.org/10.1007/s11998-020-00447-9.

Lysyk Funk, N., Leão, J., Oliveira, T., Beck, R., 2023. Semi-Solid Extrusion (SSE) in pharmaceuticals. ISBN: 978-981-9924-03-5, pp. 171–200. http://dx.doi.org/10.1007/978-981-99-2404-2_5.

Malkin, A.Y., Derkach, S.R., Kulichikhin, V.G., 2023. Rheology of Gels and Yielding Liquids. Gels 9 (9), 715. http://dx.doi.org/10.3390/gels9090715.

Matas, A., Molina-Montero, M.d.C., Igual, M., García-Segovia, P., Martínez-Monzó, J., 2022. Printability Prediction of Three Gels for 3D Food Printing. Biol. Life Sci. Forum 18 (1), 25. http://dx.doi.org/10.3390/Foods2022-12986.

Matas, A., Molina-Montero, C., Igual, M., García-Segovia, P., Martínez-Monzó, J., 2023. Viability Study on the Use of Three Different Gels for 3D Food Printing. Gels 9 (9), 736. http://dx.doi.org/10.3390/gels9090736.

Müller, M., Fisch, P., Molnar, M., Eggert, S., Binelli, M., Maniura-Weber, K., Zenobi-Wong, M., 2020. Development and thorough characterization of the processing steps of an ink for 3D printing for bone tissue engineering. Mater. Sci. Engi. C 108, 110510. http://dx.doi.org/10.1016/j.msec.2019.110510.

Nishinari, K., Fang, Y., 2018. Perception and measurement of food texture: Solid foods. J. Texture Stud. 49 (2), 160–201. http://dx.doi.org/10.1111/jtxs.12327.

Onsawai, P., Phetpan, K., Khurnpoon, L., Sirisomboon, P., 2021. Evaluation of physiological properties and texture traits of durian pulp using near-infrared spectra of the pulp and intact fruit. Measurement 174, 108684. http://dx.doi.org/10.1016/j.measurement.2020.108684.

Osswald, T., Rudolph, N., 2014. Polymer Rheology. Carl Hanser Verlag GmbH & Co. KG, pp. I–XI. http://dx.doi.org/10.3139/9781569905234.fm.

Prasetyono, T.O.H., Adhistana, P., 2019. Laboratory Study on Injection Force Measurement on Syringe and Needle Combinations. Malaysian J. Med. Sci. MJMS 26 (2), 66–76. http://dx.doi.org/10.21315/mjms2019.26.2.8.

Pstras, L., 2016. Valsalva manoeuvre using a syringe: Physics and implications. Emergency Med. J. 33 (11), 831. http://dx.doi.org/10.1136/emermed-2016-206318.

Ramli, N.A., Adam, F., Mohd Amin, K.N., Nor, A.M., Ries, M.E., 2023. Evaluation of mechanical and thermal properties of carrageenan/hydroxypropyl methyl cellulose hard capsule. Can. J. Chem. Eng. 101 (3), 1219–1234. http://dx.doi.org/10.1002/cjce.24595.

Ren, S., Tang, T., Bi, X., Liu, X., Xu, P., Che, Z., 2023. Effects of pea protein isolate on 3D printing performance, nutritional and sensory properties of mango pulp. Food Biosci. 55, 102994. http://dx.doi.org/10.1016/j.fbio.2023.102994.

Ribeiro, A., Blokzijl, M.M., Levato, R., Visser, C.W., Castilho, M., Hennink, W.E., Vermonden, T., Malda, J., 2017. Assessing bioink shape fidelity to aid material development in 3D bioprinting. Biofabrication 10 (1), 014102. http://dx.doi.org/10.1088/1758-5090/aa90e2.

Robinson, T.E., Hughes, E.A.B., Eisenstein, N.M., Grover, L.M., Cox, S.C., 2020. The quantification of injectability by mechanical testing. J. Vis. Exp. (159), 61417. http://dx.doi.org/10.3791/61417.

Rodríguez-Herrera, V.V., Umeda, T., Kozu, H., Sasaki, T., Kobayashi, I., 2024. Printability of nixtamalized corn dough during screw-based three-dimensional food printing. Foods 13 (2), 293. http://dx.doi.org/10.3390/foods13020293.

Saleh Alghamdi, S., John, S., Roy Choudhury, N., Dutta, N.K., 2021. Additive Manufacturing of Polymer Materials: Progress, Promise and Challenges. Polymers 13 (5), 753. http://dx.doi.org/10.3390/polym13050753.

Seoane-Viaño, I., Januskaite, P., Alvarez-Lorenzo, C., Basit, A.W., Goyanes, A., 2021. Semi-solid extrusion 3D printing in drug delivery and biomedicine: Personalised solutions for healthcare challenges. J. Control. Release 332, 367–389. http://dx.doi.org/10.1016/j.jconrel.2021.02.027.

Temirel, M., Dabbagh, S., Tasoglu, S., 2022. Shape Fidelity Evaluation of Alginate-Based Hydrogels through Extrusion-Based Bioprinting. J. Functional Biomater. 13 (4), http://dx.doi.org/10.3390/jfb13040225.

Thang, N.H., Chien, T.B., Cuong, D.X., 2023. Polymer-based hydrogels applied in drug delivery: an overview. Gels 9 (7), 523. http://dx.doi.org/10.3390/gels9070523.

Theagarajan, R., Moses, J.A., Anandharamakrishnan, C., 2020. 3D extrusion printability of rice starch and optimization of process variables. Food Bioprocess Technol. 13 (6), 1048–1062. http://dx.doi.org/10.1007/s11947-020-02453-6.

Varela, H., Barluenga, G., Perrot, A., 2023. Extrusion and structural build-up of 3D printing cement pastes with fly ash, nanoclays and VMAs. Cem. Concr. Compos. 142, 105217. http://dx.doi.org/10.1016/j.cemconcomp.2023.105217.

Venkatachalam, A., Balasubramaniam, A., Wilms, P.F.C., Zhang, L., Schutyser, M.A.I., 2023. Impact of varying macronutrient composition on the printability of pea-based inks in extrusion-based 3D food printing. Food Hydrocolloids 142, 108760. http://dx.doi.org/10.1016/j.foodhyd.2023.108760.

Zhou, X., Li, Z., Fan, M., Chen, H., 2013. Rheology of semi-solid fresh cement pastes and mortars in orifice extrusion. Cem. Concr. Compos. 37, 304–311. http://dx.doi.org/10.1016/j.cemconcomp.2013.01.004.

Zhu, S., Stieger, M.A., van der Goot, A.J., Schutyser, M.A.I., 2019. Extrusion-based 3D printing of food pastes: Correlating rheological properties with printing behaviour. Innovative Food Sci. Emerg. Technol. 58, 102214. http://dx.doi.org/10.1016/j.ifset.2019.102214.

Zidan, A., Alayoubi, A., Coburn, J., Asfari, S., Ghammraoui, B., Cruz, C.N., Ashraf, M., 2019. Extrudability analysis of drug loaded pastes for 3D printing of modified release tablets. Int. J. Pharm. 554, 292–301. http://dx.doi.org/10.1016/j.ijpharm.2018.11.025.

Zu, S., Wang, Z., Zhang, S., Guo, Y., Chen, C., Zhang, Q., Wang, Z., Liu, T., Liu, Q., Zhang, Z., 2022. A bioinspired 4D printed hydrogel capsule for smart controlled drug release. Mater. Today Chem. 24, 100789. http://dx.doi.org/10.1016/j.mtchem.2022.100789.